IEEE Sensors Council

Transient Response of Ion-Selective Potentiometric Wearable/Implantable Sensors

Leandro Julian Mele, M. A. Alam, *Fellow, IEEE*, and Pierpaolo Palestri, *Senior Member, IEEE*

***Abstract*— Laboratory-based potentiometric electrochemical sensors, supported by well-developed steady-state theory, have traditionally relied on endpoint detection to determine analyte concentration in various applications in agriculture, food safety, and pharmaceutical quality control, among others. In contrast, the emerging applications of wearable and implantable sensors suggest a new paradigm for real-time, continuous monitoring of analytes, for example, in healthcare and environmental monitoring. This paper develops a new analytical model for the transient response of the sensors and explains how sensor geometry, placement, and chemical properties determine the response delay. The model offers a transparent approach to optimizing sensor response, and therefore, the work would be of broad interest to sensors and system designers of not only wearable/implantable sensors, but also of modern genome-sequencers.**

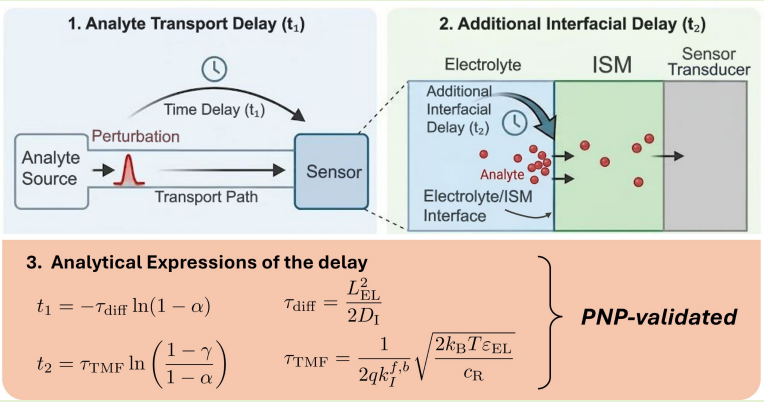

***Index Terms*— Sensors, Modeling, Wearable electronics**

I. Introduction: Transient Response of Electrochemical Sensors

THE transition from laboratory-based endpoint sensors to massively parallel sensors for genomics [1] and proteomics, as well as ubiquitous deployment of wearable and implantable sensors [2] with continuous monitoring of analytes such as glucose and nitrates, has revived practical interest in the time response of various types of potentiometric [3]–[5] and amperometric sensors [6], [7].The time responses are characterized by: (a) the delay between the analyte fluctuation and the time needed for the sensor to register it, (b) the limits of detection in a time-varying system, with the sensor delay defining the lower limit of a sensor's ability to track the time-varying analyte concentration, and (c) the characteristic features of the waveform that reflect the biochemical systems that underlie the analyte production, in other words, the ability to infer the waveform of the target analyte concentration waveform from the delayed, distorted, convoluted voltage waveform of the sensor.

In this paper, we develop a highly accurate transient model for potentiometric ISM sensors, which are widely used for water quality monitoring, quality control in the pharmaceutical industry, precision agriculture, and other applications. The approximate transient solution of the ISM, in response to an abrupt concentration change at the fluid/ISM interface, has been considered by several groups [3]; however, these analyses fail to address the delay due to transport between the analyte and the sensor, e.g., the delay between the increase in glucose concentration in blood and the corresponding response of microneedles spatially separated from blood [6].

The formulation discussed in this paper shows that, depending on the spatial separation, the reaction-dominated transient response differs fundamentally compared to that of diffusion-limited transient response, and the transition between the two regimes is described by several non-intuitive features of analyte diffusion in the fluid, concentration build-up at the fluid/ISM interface, and subsequent diffusion within the ISM membrane. The analytical results provide deep insights into the transient dynamics of ISM sensors and are validated by comparison with the Poisson-Nernst-Planck (PNP) solution. The analysis presented here complements other works on the delay of ISM-based potentiometric sensors employing finite difference descriptions of ion transport alternative to PNP [8]–[10].

It should be noted that the response times analyzed in this work reflect the fundamental electrochemical delay of the sensor, distinct from any additional system-level delays introduced by the acquisition electronics,that is not analyzed in the present work.

The paper is organized as follows. Section II defines the

L. J. Mele is with the Department of Materials Science and Engineering, Stanford University, Stanford, California 94305, USA.

M. A. Alam is with the School of Electrical and Computer Engineering, Purdue University, West Lafayette, Indiana 47907, USA.

P. Palestri is with the Engineering Department "Enzo Ferrari", University of Modena and Reggio Emilia, Modena, 41125, Italy.

model system and summarizes its transient response by using the PNP model. Section III-V, respectively, develop the analytical theory of the transient response for diffusion-limited, reaction-limited, and reaction-diffusion-limited sensors. The conclusions are summarized in Section VI of the paper. The details of the derivations are in the Appendices.

II. Definition of the Problem and PNP Model

The Ion-Sensitive-Electrode (ISE) considered in this work as potentiometric sensor is composed of a Ion-Selective-Membrane (ISM) and the solid electrode. Fig. 1 shows an ISE immersed in the fluid containing the analyte. The ISM is composed of a hydrophobic plasticized polymeric matrix (typically high-molecular-weight poly(vinyl chloride)) doped with fixed Anionic Sites (R^-). To ensure permselectivity, the ISM contains a lipophilic ion-exchanger, such as potassium tetrakis(p-chlorophenyl)borate ($c_{\mathrm{R}} = 100$ mM in this model). These negative sites are covalently or sterically trapped within the organic matrix, providing the necessary charge compensation for the incoming primary cations.

At time $t = 0$, the concentration of an 1:1 salt (I^+-X^-) is modified at a distance L_{EL} from the ISM/electrolyte junction [11] located at $z = 0$. The analyte is allowed to diffuse towards the electrode/ISM interface. At the interface, the permselective ISM allows the ion I^+ to enter the membrane, and blocks the counter-ion X^- (Donnan exclusion [12]). This establishes the analytical model's range of validity, which strictly requires the Nernstian regime ($c_{\mathrm{R}} \gg c_{\mathrm{B}}$) to ensure perfect Donnan exclusion. Although the numerical PNP model can compute non-Nernstian dynamics, such regimes fall outside the scope of the analytical framework presented in this work. Once primary ions I^+ transfer into the membrane, the transport through the membrane occurs under the combined influence of drift and diffusion. The process continues until equilibrium is achieved.

First, let us analyze the problem using a physics-based numerical simulator [11] to create a set of reference results. The simulator self-consistently solves the Poisson–Nernst–Planck (PNP) equations for ion transport coupled with Chang-Jaffé boundary conditions [13] to describe the ion transfer kinetics at the electrolyte/ISM interface. Given the planar geometry sketched in Fig. 1, where the concentration change is assumed to be uniform across the plane parallel to the ISM, ion transport is dominated by diffusion and drift perpendicular to the interface. A 1D model is therefore sufficient to capture the essential dynamics of the sensor's transient response. In terms of practical implementations, the most directly relevant systems respecting this quasi-1D geometry are microfluidic devices, where the channel cross-section aligns with the sensor [14]. Although direct experimental measurements probing the response time in this specific architectural regime are currently lacking, the numerical PNP framework employed here to validate our analytical derivations has been thoroughly calibrated against experimental data. Specifically, the model accurately reproduces both experimental steady-state membrane potentials across varying ion concentrations [15] and the dynamic response characteristics of practical potentiometric sensors [11].

Unless specified otherwise, the PNP simulator uses the default physical constants, transport parameters, and boundary conditions summarized in Table I.

TABLE I
DEFAULT NUMERICAL PARAMETERS AND BOUNDARY CONDITIONS FOR THE PNP SIMULATOR.

Parameter	Symbol/Type	Value / Condition
Physical Parameters		
Temperature	T	298 K
Permittivity (Electrolyte)	$\varepsilon_{\mathrm{EL}}$	80
Permittivity (Membrane)	$\varepsilon_{\mathrm{ISM}}$	5
Layer Thicknesses	L	100 μm
Fixed Site Conc.	c_{R}	100 mM
Diff. Coeff. (Electrolyte)	D_{EL}	1×10^{-9} m^2/s
Diff. Coeff. (Membrane)	D_{ISM}	1×10^{-11} m^2/s
Boundary Conditions		
Bulk Electrolyte ($z = -L_{\mathrm{EL}}$)	Dirichlet	$\psi = 0$ V $c_i = c_{\mathrm{B}}$
Interface Rates ($z = 0$)	Chang-Jaffé	$k_{\mathrm{I}}^{f,b}$ k_{X}=0
Bulk Membrane ($z = L_{\mathrm{ISM}}$)	Neumann	Null flux ($\nabla\psi = 0, \mathbf{J}_i = 0$)

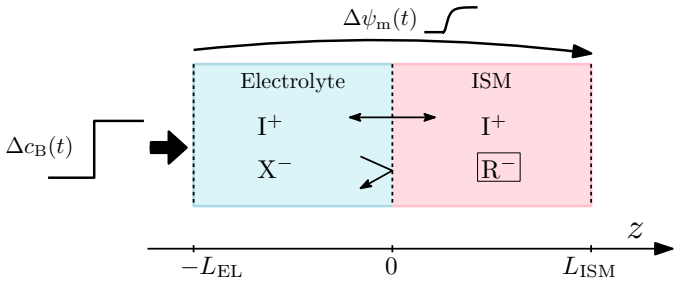

Fig. 1. Sketch of the ISE consisting of an electrolyte and an ISM. Cations, I^+, are exchanged between phases (ISM and electrolyte) and compensate the ionic sites of the ISM, whereas counter-ions, X^-, are excluded from the ISM. A perturbation of the ionic concentration in the bulk of the electrolyte at a distance L_{EL} from the electrolyte/ISM junction (set as $z = 0$) propagates to the membrane and generates a change in the membrane potential ψ_{m}.

For an insight into the distinct transport phases, Fig. 2 summarizes the transport response of an ISM obtained by using the PNP numerical simulator. Here, at time $t = 0$ the concentration of both I^+ and X^- changes from c_{B1} to c_{B2}. The transient consists of two phases:

- A *diffusion-limited* regime where the perturbation in the bulk of the electrolyte propagates towards the interface with the ISM; the membrane potential remains constant during the short initial phase of this regime (profiles 1-3 in Fig. 2.a); then, the concentration in proximity to the junction changes from c_{B1} to c_{B2} followed by flattening of the concentration profile in the electrolyte ($c_{\mathrm{I}} = c_{\mathrm{X}} = c_{\mathrm{B2}}$) (up to profile 6 in Fig. 2.a); during this time, the membrane potential changes but it does not reach the equilibrium value expected from Nernst's law.
- A *trans-membrane flux-limited* regime is dictated by the transfer of ions between the ISM and the electrolyte to

maintain overall charge neutrality after the modification of the surface potential. During this regime, the concentration overshoot at the EL/ISM interface lowers to an equilibrium value (profiles 6 to 8 in Fig. 2.a) while the membrane potential attains the equilibrium value as shown in Fig. 2b.

In the next section, we will derive analytical models for the two phases and their relative contribution to the overall delay of the sensor response.

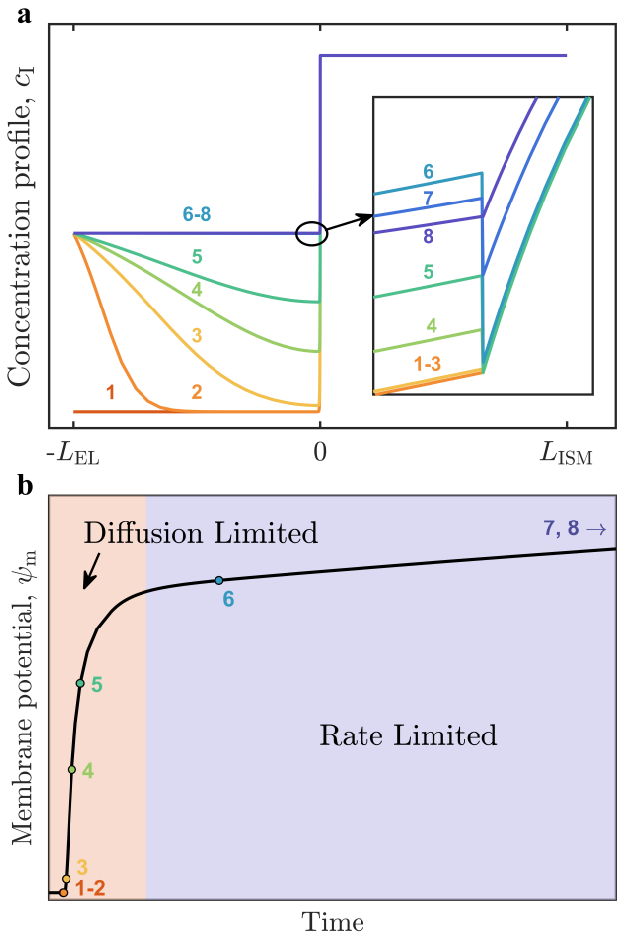

Fig. 2. (a) Cation concentration profiles in the EL/ISM system at different times after a concentration step change in the bulk of the electrolyte. (b) Resulting membrane potential vs time.

III. Model for the Diffusion-Limited Regime

During the diffusion-limited regime, the evolution of the system is driven by the diffusion of ion I^+, along with its counter-ion X^-. When ions have equal diffusivities, electroneutrality is maintained, and it is possible to neglect the electric field in the electrolyte and solve the diffusion equation only

$$\frac{\partial c_I}{\partial t} = D_I \frac{\partial^2 c_I}{\partial z^2}. \tag{1}$$

Equation (1) is linear and can be solved for the change of concentration Δc_B with respect to the initial value c_{B1}. Assuming the concentration change of $c_I(-L_{EL})$ from c_{B1} to c_{B2} to be instantaneous, and momentarily neglecting the presence of the ISM, (1) has analytical solution in the form

$$c_I(z,t) = c_{B1} + (c_{B2} - c_{B1}) \cdot \mathrm{erfc}\left\{\frac{z + L_{EL}}{\sqrt{4D_I t}}\right\}, \tag{2}$$

which describes the propagation of the perturbation from $z = -L_{EL}$ to ∞.

Introduction of the ISM at $z = 0$. [1] If the charge transfer at the junction is much slower than the diffusion (that is always true for realistic values of transfer rates), the flux of ions at $z = 0$ can be considered as essentially null, i.e., the ISM resembles a hard wall during the diffusion time-scales. We can thus write:

$$\frac{\partial c_I}{\partial z}(0) \approx 0. \tag{3}$$

This boundary condition can be enforced in the solution of (1) by using the method of the images, i.e., considering a mirrored erfc function propagating from $z = L_{EL}$. Normalization is then needed to ensure that $c_I(z = -L_{EL}, t > 0) = c_{B2}$, leading to

$$c_I(z,t) = c_{B1} + (c_{B2} - c_{B1}) \frac{\mathrm{erfc}\left\{\frac{z+L_{EL}}{\sqrt{4D_I t}}\right\} + \mathrm{erfc}\left\{\frac{L_{EL}-z}{\sqrt{4D_I t}}\right\}}{1 + \mathrm{erfc}\left\{\frac{2L_{EL}}{\sqrt{4D_I t}}\right\}}. \tag{4}$$

Fig. 3 (a) demonstrates the excellent match between (4) and reference results from the PNP simulator.

By defining the dimensionless quantities

$$\zeta^+ = \frac{1 + z/L_{EL}}{\sqrt{2t/\tau}}$$
$$\zeta^- = \frac{1 - z/L_{EL}}{\sqrt{2t/\tau}}, \tag{5}$$

with,

$$\tau = \frac{L_{EL}^2}{2D_I} \tag{6}$$

one can rewrite (4) in a compact form as

$$\frac{c_I - c_{B1}}{c_{B2} - c_{B1}} = \frac{\mathrm{erfc}\{\zeta^+\} + \mathrm{erfc}\{\zeta^-\}}{1 + \mathrm{erfc}\{\zeta^+ + \zeta^-\}}. \tag{7}$$

Equation (7) explains the evolution of the ion concentration in the electrolyte during the diffusion-limited phase.

The concentration of ion species I^+ in proximity of the interface, i.e., $c_{ITF}(t) = c_I(0^-, t)$, allows one to calculate the time-dependent membrane potential by using the Nernst relation:

$$\psi_m(t) = V_{th} \ln \frac{c_{ITF}(t)}{c_R}, \tag{8}$$

where $V_{th} = k_B T/q$ is the thermal voltage.

Remarkably, (7) evaluated at the EL/ISM interface ($z = 0$) can also be approximated by an exponential function shifted by a time t_1:

$$c_{ITF}(t) = c_{B1} + (c_{B2} - c_{B1}) \left[1 - \exp -\frac{t - t_1}{\tau}\right]. \tag{9}$$

[1] To be precise, we indicate with 0 not the junction itself but the left side of the built-in field region associated with the junction. We assume here that the field region is much thinner than the diffusion region. The presence of ISM at $z = 0$ requires us to account for the transmitted and the reflected ion fluxes.

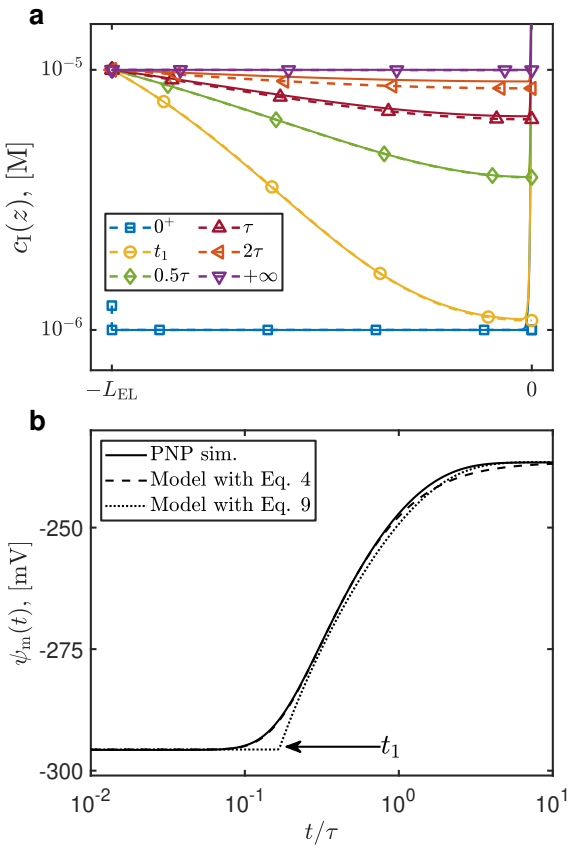

Fig. 3. (a) Time evolution of the concentration profile of ion I^+ during the diffusion-limited phase according to (7) (dashed lines with symbols) and PNP simulations (solid lines) for different time snapshots as a function of τ. and (b) comparison of the time-dependent membrane potential using PNP (solid line) and either (9) plus (8) (dotted) or (4) plus (8) (dashed). Note that the solutions correspond to the diffusion-dominated regime shown in Fig. 2.

We have verified that the empirical assumption $t_1 = \tau/6$ holds across a wide range of parameter values. Our results show that t_1 is the time needed for the ionic profile to pass from profile '1' to profile '3' in Fig. 2(a), which corresponds to the onset of membrane potential change (dashed vertical line in Fig. 2(b)).

Fig. 3 (bottom) shows that (8) using either the exact (7) or the approximated (9), correctly reproduce the PNP results in terms of $\psi_{\rm m}(t)$.

In the diffusion-limited regime, the analytical model predictions compare well to PNP simulations, see Fig. 4. In these simulations, the ISM parameters are chosen to make the contribution to the delay from the transmembrane flux negligible.

IV. The Trans-Membrane Flux Limited Regime

The model proposed in the previous section reproduces the sensor response when $L_{\rm EL}$ is large and when $k_{\rm I}^f$ and $k_{\rm I}^b$ are large as well (what we mean by *large* will be clear in the following). In these situations, diffusion of the ion I^+ dominates. When $L_{\rm EL}$ is short and/or transfer rates are low, transmembrane ion transport becomes dominant, and the delay becomes independent of $L_{\rm EL}$. Unlike the diffusion-dominated region, the flux-dominated regime is dictated by the interface

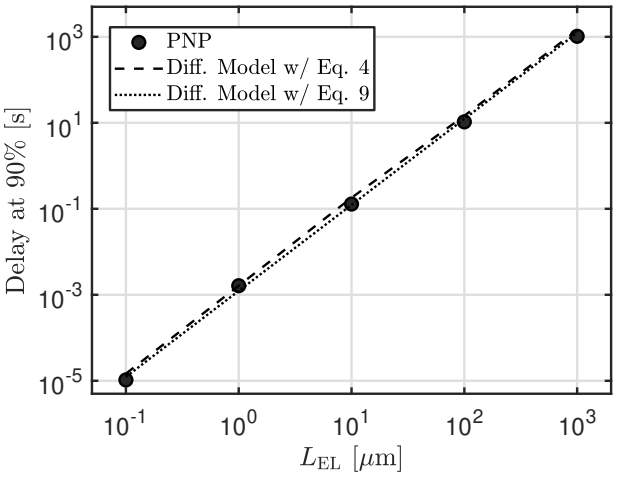

Fig. 4. Response delay to a $\Delta c_{\rm B}$ change from 100 to 110 μM vs the electrolyte thickness, derived from numerical PNP simulations (symbols) and using (7) plus (8) (dashed line). $k_{\rm I}^f = k_{\rm I}^b = 10^{-4}$ m/s.

electric field, $F(0^-)$ and $F(0^+)$ at the two sides of the junction, and can be calculated as follows.

A. Quasi-static analysis

We follow a quasi-static approximation to compute the change in the charge in the ISM region when the electrolyte bulk changes from $c_{\rm B1}$ to $c_{\rm B2}$. For details, see Appendix I. Compared to the general derivation provided therein, here we assume that the membrane doping $c_{\rm R}$ is much higher than the bulk ion concentration, so that the transition region (with a non-zero electric field) is restricted to the electrolyte side, whereas the ISM potential profile is essentially flat. Let us also assume that $c_{\rm I}(z=0) \approx c_{\rm R}$ (the time variable is dropped in this quasi-static analysis, so that all quantities only depend on the position z).

We substitute (26) into (25), set $a = -L_{\rm EL}$ and $b = 0$, and then apply boundary conditions $F(a) = 0$ V/m, $\psi(a) = 0$ V, and $\psi(b) = (k_{\rm B}T/q)\ln(c_{\rm B}/c_{\rm R})$, to finally obtain the field at the electrolyte side of the interface:

$$|F(0^-)| = \sqrt{\frac{2k_{\rm B}T}{\varepsilon_{\rm EL}}}\left(\sqrt{c_{\rm R}} - \frac{c_{\rm B}}{\sqrt{c_{\rm R}}}\right). \tag{10}$$

Applying Gauss's law ($Q_{\rm ISM} = -\varepsilon_{\rm EL}F(0^-)$), the charge in the ISM is:

$$Q_{\rm ISM} = -\sqrt{2k_{\rm B}T\varepsilon_{\rm EL}}\left(\sqrt{c_{\rm R}} - \frac{c_{\rm B}}{\sqrt{c_{\rm R}}}\right). \tag{11}$$

If $c_{\rm B}$ changes by $\Delta c_{\rm B} = c_{\rm B2} - c_{\rm B1}$, the change in ISM charge is

$$\frac{\Delta Q_{\rm ISM}}{\Delta c_{\rm B}} \approx \frac{dQ_{\rm ISM}}{dc_{\rm B}} = \sqrt{\frac{2k_{\rm B}T\varepsilon_{\rm EL}}{c_{\rm R}}}, \tag{12}$$

i.e., the charge in the ISM becomes less negative as $c_{\rm B}$ increases. The shape of the potential profiles and charges for the different bulk concentrations in steady-state is sketched in Fig. 5.a.

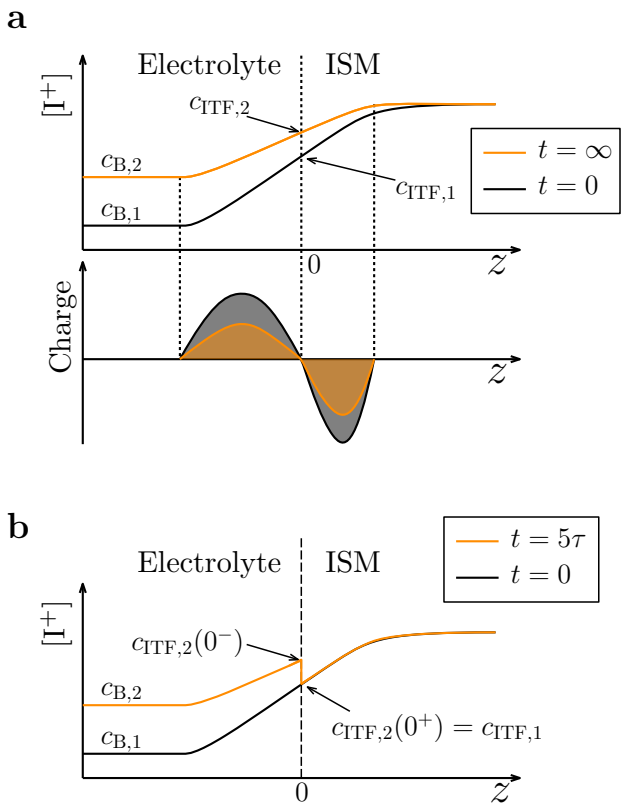

Fig. 5. a) Quasi-static view of the EL/ISM junction before and after changing the bulk electrolyte concentration. b) Sketch of concentration profile of ion I^+ in case of rate-limited response at the beginning of the transient.

B. Time evolution of the interface concentration

If we assume that diffusion in the electrolyte is not the limiting factor and it is quite fast compared to trans-membrane fluxes, at $t \simeq 0$ (that means close to $\simeq 5\tau$, i.e., the delay of the diffusion phase) the interface concentration at the electrolyte side $c_{\mathrm{ITF}}(z = 0^-, t \simeq 0)$ would change quite instantaneously[2], see Fig. 5.b. According to the derivation shown in Appendix III, the change in $c_{\mathrm{ITF}}(0^-, t)$ when the bulk concentration changes by Δc_{B} is roughly $2\Delta c_{\mathrm{B}}$. The concentration $c_{\mathrm{ITF}}(0^+, t)$ will then change as well, since at the end of the transient $c_{\mathrm{I}}(0^+, t \to \infty)$ and $c_{\mathrm{I}}(0-, t \to \infty)$ should be equal. The trans-membrane flux (from electrolyte to ISM) is thus

$$\mathcal{F}_{\mathrm{ISM}}(t) = c_{\mathrm{ITF}}(0^-, t)k_I^f - c_{\mathrm{ITF}}(0^+, t)k_I^b = -k_I^{f,b}\Delta c_{\mathrm{ITF}}(0^+, t). \tag{13}$$

The fluxes change over time because the concentrations on both sides tend to the same value, see Fig. 2. Let us first consider the total charge to be transferred across the membrane and the flux at time $t = 0$[3] and define a suitable time constant for the Trans-Membrane-Flux limited delay:

$$\tau_{\mathrm{TMF}} \approx -\frac{\Delta Q_{\mathrm{ISM}}}{q\mathcal{F}_{\mathrm{ISM}}(0)}. \tag{14}$$

By using (13), we can rewrite it as:

$$\tau_{\mathrm{TMF}} \approx \frac{\Delta Q_{\mathrm{ISM}}}{\Delta c_{\mathrm{B}}} \frac{\Delta c_{\mathrm{B}}}{qk_{\mathrm{I}}^{f,b}\Delta c_{\mathrm{ITF}}(0^+, 0)} \tag{15}$$

Using (12) and considering that (see Appendix III), $\Delta c_{\mathrm{ITF}}(0^+, 0) \approx 2\Delta c_{\mathrm{B}}$, we get

$$\tau_{\mathrm{TMF}} \approx \frac{1}{2qk_I^{f,b}} \sqrt{\frac{2k_{\mathrm{B}}T\varepsilon_{\mathrm{EL}}}{c_{\mathrm{R}}}}. \tag{16}$$

Fig. 6 shows that τ_{TMF} accurately reproduces the response of ISM dominated by the trans-membrane fluxes. For simplicity, we have assumed $k_{\mathrm{I}}^f = k_{\mathrm{I}}^b$.

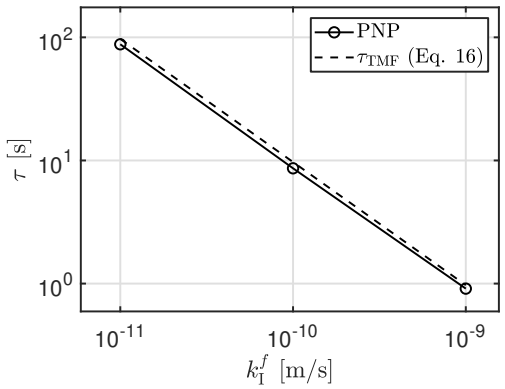

Fig. 6. Comparison of rate-limited (RL) time constant delay from PNP simulations vs t_{TMF} from (16). PNP time constant was calculated as $t_{90}/\ln 10$, with t_{90} the time to reach 90% of the membrane potential excursion after the diffusion delay (see Fig. 7).

V. Combined Effect of Trans-Membrane Flux and Ion Diffusion in the Electrolyte

The transient response is a complex interplay between the two processes of ion diffusion in the electrolyte and trans-membrane fluxes at the EL/ISM junction. As shown in Fig. 7, the total change in membrane potential, $\Delta\psi_{\mathrm{tot}}$, does not occur entirely within one phase. Instead, it is partitioned between a fast initial change during the diffusion-limited phase, $\Delta\psi_{\mathrm{diff}}$, and a subsequent, slower change during the kinetic-limited phase, $\Delta\psi_{\mathrm{kin}} = \Delta\psi_{\mathrm{tot}} - \Delta\psi_{\mathrm{diff}}$.

To develop a comprehensive model, we must first determine how this potential drop is split. This partitioning is dictated by the equilibrium (i.e., before the application of the Δc_{B} step) electrostatic potential, ψ_0, at the EL/ISM interface relative to the bulk. As detailed in Appendix I, ψ_0 is determined by solving the Poisson-Boltzmann equation for the system. While the exact value is found via the transcendental equation Equation 29, a compact approximation useful for modeling is:

$$\psi_0 \approx \frac{\psi_{\mathrm{m}}}{1 + 2\frac{\varepsilon_{\mathrm{EL}}c_{\mathrm{B}}}{\varepsilon_{\mathrm{ISM}}c_{\mathrm{R}}}}, \tag{17}$$

[2]in the previous calculation we set it to $\approx c_{\mathrm{R}}$ but it would be a little bit lower and should change when the bulk concentration changes, as discussed in Section I.

[3]If applied to the discharge of a capacitor C over a resistor R this method would give $\tau_{RC} = Q/I(0) = CV(0)/[V(0)/R] = RC$, that is the correct expression for the time constant of the RC circuit.

where ψ_{m} is the total equilibrium membrane potential. We note that the model imposes no theoretical limits on the magnitude of ψ_0.

We determine the split of the potential drop during the transient by applying a perturbation analysis to this equilibrium state, as derived in Appendix II. The fraction of the total potential change that occurs during the diffusion-limited regime, denoted as $\gamma = |\Delta\psi_{\mathrm{diff}}/\Delta\psi_{\mathrm{m}}|$, is given by:

$$\gamma = \tanh\left(\frac{\psi_0}{2V_{\mathrm{th}}}\right). \tag{18}$$

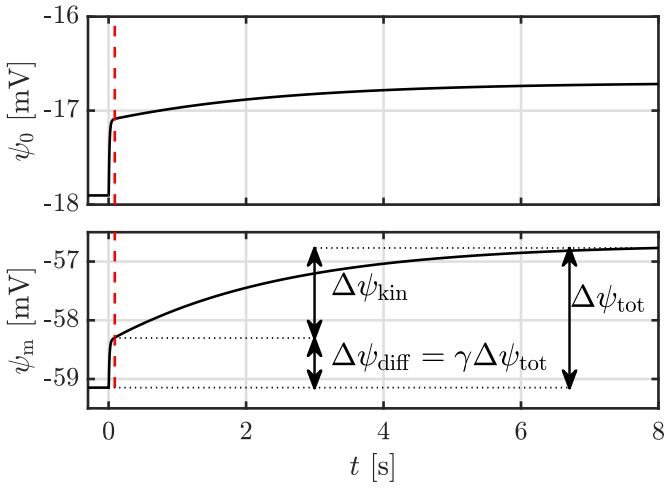

Fig. 7. Transient response of interfacial and membrane potentials. The temporal evolution of the potential at the electrolyte/membrane interface ψ_0 (top panel) and the membrane potential ψ_{m} (bottom panel) following a bulk concentration step of the primary ion I^+ from 1 mM to 1.1 mM. The vertical red dashed line marks the theoretical end of the diffusion limited phase. Simulation parameters: Electrolyte thickness $d_{\mathrm{el}} = 5$ μm; Ionic sites concentration $c_{\mathrm{R}} = 10$ mM; Interfacial kinetic transfer rate $k_{\mathrm{I}}^{f,b} = 10^{-9}$ m/s.

This parameter, γ, characterizes diffusion-limited vs. kinetic-limited contributions to the sensor response. The validity of (18) is confirmed by comparing it against the numerical PNP simulations, as shown in Fig. 8. The model accurately captures the transition of the potential split factor γ across a wide range of bulk concentrations (c_{B1}), membrane site densities (c_{R}), and dielectric constants ($\varepsilon_{\mathrm{ISM}}$).

We can now compare the expressions derived before for general cases with different electrolyte thicknesses and ISM parameters. To quantify the boundary between the diffusion-dominated and flux-dominated regimes, we introduce the dimensionless number χ, defined as the ratio of the characteristic diffusion time to the transmembrane flux time:

$$\chi \equiv \frac{\tau_{\mathrm{diff}}}{\tau_{\mathrm{TMF}}} = \frac{k_{\mathrm{I}}^{f,b} L_{\mathrm{EL}}^2}{D_{\mathrm{I}}} \sqrt{\frac{q^2 c_{\mathrm{R}}}{2k_{\mathrm{B}}T\varepsilon_{\mathrm{EL}}}}. \tag{19}$$

The transition occurs when $\chi \approx 1$. This allows us to define a critical electrolyte thickness, L_{crit}, below which the sensor response becomes rate-limited:

$$L_{\mathrm{crit}} = \sqrt{\frac{D_{\mathrm{I}}}{qk_I}} \sqrt{\frac{2k_{\mathrm{B}}T\varepsilon_{\mathrm{EL}}}{c_{\mathrm{R}}}}. \tag{20}$$

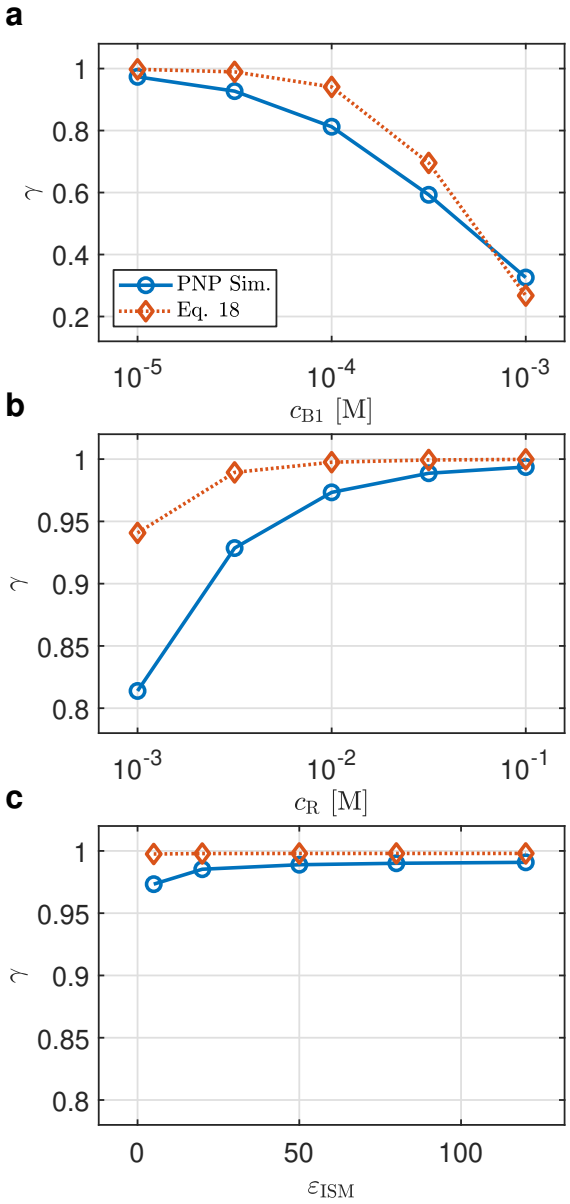

Fig. 8. Validation of the analytical model for the potential split factor γ. **a)** Sweep of bulk concentration c_{B1} (with $c_{\mathrm{R}} = 10$ mM and $\varepsilon_{\mathrm{ISM}} = 5$). **b)** Sweep of fixed ionic site concentration c_{R} (with $c_{\mathrm{B1}} = 10$ μM). **c)** Sweep of membrane dielectric constant $\varepsilon_{\mathrm{ISM}}$ (with $c_{\mathrm{B1}} = 10$ μM and $c_{\mathrm{R}} = 10$ mM). PNP simulation results (solid lines with circles) show excellent agreement with predictions from (18). In all cases, $\Delta c_{I,B}$ of 10% of c_{B1} was used.

The results are reported in Fig. 9. The dotted lines represent the diffusion delay, calculated as:

$$t_{\mathrm{diff}} = -\tau_{\mathrm{diff}} \ln(1-\alpha), \tag{21}$$

where α is the fraction of the membrane potential change when we consider the transient to be over.

In Fig. 9.a, the ISM parameters are selected so that the potential split factor γ is small. For $\chi \gg 1$ (i.e., $L_{\mathrm{EL}} \gg L_{\mathrm{crit}}$), the transmembrane transport is faster than diffusion. Consequently, diffusion is the limiting factor and (21) accurately reproduces the results. Conversely, when $\chi \ll 1$ (i.e., $L_{\mathrm{EL}} \ll L_{\mathrm{crit}}$), the delay from PNP simulations becomes flat and

independent of L_{EL}. In this regime, the fast diffusion phase contributes negligibly to the total potential excursion. The remaining transient is dominated by the rate-limited transport at the interface, and the delay matches our model prediction:

$$t_{\mathrm{TMF}} = \tau_{\mathrm{TMF}} \ln \frac{1-\gamma}{1-\alpha}. \tag{22}$$

In Fig. 9.b, the parameters result in $\gamma \approx 0.82$. In this case, for the reaction-limited plateau to be observable in the sensor delay, the diffusion phase must not exceed the detection threshold. Mathematically, the reaction-limited regime appears only when $\gamma < \alpha$. Conversely, when $\gamma > \alpha$ (red curve in Fig. 9.b), the response is dominated by diffusion ($t \propto L_{\mathrm{EL}}^2$) across the entire range of thicknesses, effectively masking the transition to the reaction-limited regime.

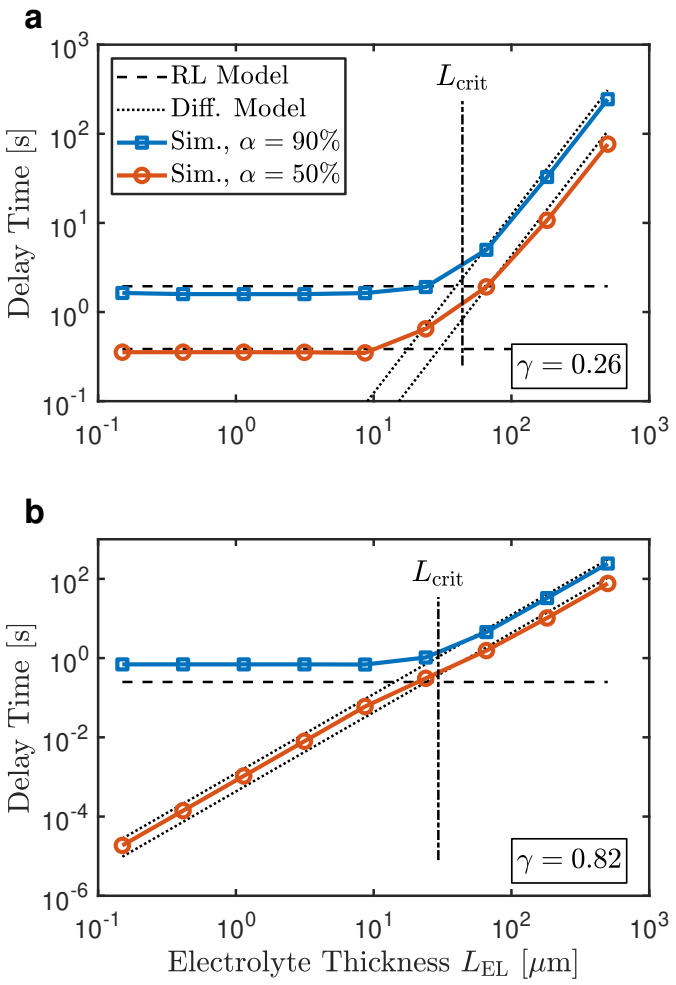

Fig. 9. Comparison of the response delay times setting $\alpha = 50\%$ (circles, red) and $\alpha = 90\%$ (squares, blue) as a function of the electrolyte thickness L_{EL} for **a** a low γ and **b** a high γ regime (reported in the figures using (17) and (18)). Solid lines with symbols represent the numerical PNP simulation results. The dashed lines represent the Reaction-Limited (RL) analytical model ((22)) and the dotted lines represent the Diffusion-Limited model ((21)), which dominates for large L_{EL}. Key simulation parameters: interfacial transfer rate $k_{\mathrm{I}}^{f,b} = 10^{-8}$ m/s, bulk electrolyte concentration $c_{\mathrm{I,B}} = 100$ μM with $\Delta c_{\mathrm{I,B}} = 10$ μM and membrane site concentration $c_{\mathrm{R}} = 1$ mM in **a** and $c_{\mathrm{R}} = 5$ mM in **b**.

The key analytical expressions derived for the diffusion-limited and rate-limited regimes, along with the coupling parameters that determine the dominant mechanism, are summarized in Table II.

TABLE II
SUMMARY OF KEY COMPACT MODEL EQUATIONS

Parameter	Equation
Diffusion-Limited Regime	
Time Constant	$\tau_{\mathrm{diff}} = \frac{L_{\mathrm{EL}}^2}{2D_{\mathrm{I}}}$
Response Delay	$t_{\mathrm{diff}} = -\tau_{\mathrm{diff}} \ln(1-\alpha)$
Reaction-Limited Regime	
Time Constant	$\tau_{\mathrm{TMF}} = \frac{1}{2qk_I^{f,b}} \sqrt{\frac{2k_{\mathrm{B}}T\varepsilon_{\mathrm{EL}}}{c_{\mathrm{R}}}}$
Response Delay	$t_{\mathrm{TMF}} = \tau_{\mathrm{TMF}} \ln\left(\frac{1-\gamma}{1-\alpha}\right)$
Transition between the two regimes	
Interface Potential	$\psi_0 \approx \frac{\psi_{\mathrm{m}}}{1+2\frac{\varepsilon_{\mathrm{EL}} c_{\mathrm{B}}}{\varepsilon_{\mathrm{ISM}} c_{\mathrm{R}}}}$
Regime Parameter	$\chi = \tau_{\mathrm{diff}}/\tau_{\mathrm{TMF}}$
Critical Length	$L_{\mathrm{crit}} = \sqrt{\frac{D_{\mathrm{I}}}{qk_I^{f,b}} \sqrt{\frac{2k_{\mathrm{B}}T\varepsilon_{\mathrm{EL}}}{c_{\mathrm{R}}}}}$ $(\gamma < \alpha)$
Split Factor	$\gamma = \tanh\left(\frac{\psi_0}{2V_{\mathrm{th}}}\right)$
Interface Overshoot	$\Delta c_{\mathrm{ITF}} \approx 2\Delta c_{\mathrm{B}}$

VI. DISCUSSION AND CONCLUSION

To summarize, the paper develops a comprehensive analytical model for the transient response of potentiometric ion-selective membrane (ISM) sensors, applicable to both diffusion-limited and transport-limited regimes. The key insights are:

- *Identification of Dual Response Regimes:* The sensor's time response is governed by two distinct physical processes: ion diffusion in the electrolyte and transmembrane ion flux at the membrane interface.
- *The Voltage Split Factor (γ):* The model introduces a critical parameter, γ (calculated as $\tanh(\psi_0/2V_{\mathrm{th}})$), which quantifies the fraction of the potential change occurring during the initial diffusion phase versus the subsequent kinetic phase.
- *Non-Intuitive Delay Scaling:* * In the diffusion-limited regime (large L_{EL}), the response delay scales with the square of the electrolyte thickness (L_{EL}^{-2}). In the reaction-limited regime (small L_{EL} and low γ), the delay becomes "flat," meaning it is independent of the electrolyte thickness and is instead dominated by interfacial transfer kinetics. In situations where γ is high, the rate-limited delay phase may not be observed, and the delay would always scale as L_{EL}^{-2}.
- *Interface Concentration Overshoot:* The paper analytically demonstrates that the concentration change at the

interface (Δc_{ITF}) can be roughly double the change in bulk concentration ($2\Delta c_{\mathrm{B}}$), a phenomenon that significantly impacts the rate-limited response.

Overall, the model provides a theoretical foundation for optimizing the response time of emerging wearable and implantable sensors, where spatial separation from the analyte makes traditional steady-state theory inadequate. Indeed, we note that the equilibrium Nernst response may take a prohibitively long time to achieve in some regimes. Consequently, the partition voltage may need to be used to calculate the actual analyte concentration rather than the final steady-state value.

Finally, we suggest several potential generalizations of the work reported here. First, the current model focuses exclusively on 1D transport. While the impact of multi-dimensional diffusive transport in 3D architectures, such as spherical or microneedle geometries, has been explored both numerically and analytically in recent literature [6], [16], [17], the rigorous 1D derivations presented here establish the fundamental dimensionless scaling variables necessary to generalize the diffusion delay (τ_{diff}) to such 3D systems. In contrast, the transmembrane flux determining τ_{TMF} occurs strictly at the local interface and thus remains a fundamentally planar phenomenon, largely independent of the macroscopic sensor geometry. Second, the theoretical framework is developed for single-ion species and assumes equal forward and backward transfer rates, yet real-world physiological environments often involve complex mixtures of ions with varying membrane affinities that could influence sensor response. Third and finally, the paper does not address time-dependent sensor degradation, such as biofouling and dopant leaching from the membrane. Future work could address the limitations identified in this paper. Finally, the calculated delays is the intrinsic electrochemical limit of the sensor interface, which serves as a lower bound for the overall system-level response time.

The analytical framework developed in this work may find application in the modeling of the time response of Organic Electrochemical Transistors (OECTs), where ion-selective membranes play a critical role in continuous multi-ion and biochemical sensing [18], [19].

Appendix I
Quasi-static Analysis and Derivation of Interface Potential

In this appendix, we detail the quasi-static analysis of the charge accumulation and the electrostatic potential at the electrolyte/ISM interface. We assume the ions to be at equilibrium.

We start by analyzing the electric field distribution. The gradient of the squared electric field F is related to the charge density ρ by:

$$\frac{dF^2}{dz} = 2F\frac{dF}{dz} = 2F\frac{\rho}{\varepsilon_{\mathrm{EL}}}. \tag{23}$$

Using the relationship between the field and the potential gradient:

$$\frac{dF^2}{dz} = -\frac{2\rho}{\varepsilon_{\mathrm{EL}}}\frac{d\psi}{dz}. \tag{24}$$

Integrating this expression from point a to point b yields:

$$F^2(b) - F^2(a) = -\frac{2}{\varepsilon_{\mathrm{EL}}}\int_{\psi(a)}^{\psi(b)} \rho(\psi)d\psi. \tag{25}$$

To determine the interface potential ψ_0, we must solve the Poisson-Boltzmann equation for both domains. The charge density in the electrolyte is given by:

$$\rho_{\mathrm{EL}}(\psi) = qc_{\mathrm{B}}\left[e^{-q\psi/k_{\mathrm{B}}T} - e^{+q\psi/k_{\mathrm{B}}T}\right]. \tag{26}$$

In the ISM, $\psi(+L_{\mathrm{ISM}}) = \psi_{\mathrm{m}} = V_{\mathrm{th}}\ln(c_{\mathrm{B}}/c_{\mathrm{R}})$, the density is:

$$\rho_{\mathrm{ISM}}(\psi) = qc_{\mathrm{R}}[e^{q(\psi_{\mathrm{m}}-\psi)/k_{\mathrm{B}}T} - 1]. \tag{27}$$

Using Gauss's law at the interface, $\varepsilon_{\mathrm{EL}}F(0^-) = \varepsilon_{\mathrm{ISM}}F(0^+)$, and evaluating the field expressions:

$$\begin{aligned} F^2(0^-) &= \frac{2k_{\mathrm{B}}Tc_{\mathrm{B}}}{\varepsilon_{\mathrm{EL}}}[e^{q\psi_0/k_{\mathrm{B}}T} + e^{-q\psi_0/k_{\mathrm{B}}T} - 2] \\ F^2(0^+) &= \frac{2k_{\mathrm{B}}Tc_{\mathrm{R}}}{\varepsilon_{\mathrm{ISM}}}[e^{q(\psi_{\mathrm{m}}-\psi_0)/k_{\mathrm{B}}T} - 1 - \frac{q}{k_{\mathrm{B}}T}(\psi_{\mathrm{m}} - \psi_0)], \end{aligned} \tag{28}$$

we arrive at the transcendental equation for ψ_0:

$$\frac{\varepsilon_{\mathrm{EL}}c_{\mathrm{B}}}{\varepsilon_{\mathrm{ISM}}c_{\mathrm{R}}} = \frac{\exp\left(\frac{\psi_{\mathrm{m}}-\psi_0}{V_{\mathrm{th}}}\right) - 1 - \frac{\psi_{\mathrm{m}}-\psi_0}{V_{\mathrm{th}}}}{\exp\left(\frac{\psi_0}{V_{\mathrm{th}}}\right) + \exp\left(-\frac{\psi_0}{V_{\mathrm{th}}}\right) - 2}. \tag{29}$$

Appendix II
Derivation of Potential Split Factor γ

This appendix details the derivation of the potential split factor γ by analyzing the perturbation of the equilibrium state derived in Appendix I.

We start with the transcendental equation (29) that governs the interface potential. We simplify the notation by defining the RHS numerator as $\mathcal{N}$ and the denominator as $\mathcal{D}$:

$$\frac{\varepsilon_{\mathrm{EL}}c_{\mathrm{B}}}{\varepsilon_{\mathrm{ISM}}c_{\mathrm{R}}} = \frac{\mathcal{N}(\psi_{\mathrm{m}} - \psi_0)}{\mathcal{D}(\psi_0)}, \tag{30}$$

where $\mathcal{N}(x) = e^{x/V_{\mathrm{th}}} - 1 - x/V_{\mathrm{th}}$ and $\mathcal{D}(y) = e^{y/V_{\mathrm{th}}} + e^{-y/V_{\mathrm{th}}} - 2$.

We consider the perturbation in the bulk concentration $c_{\mathrm{B}} \to c_{\mathrm{B}} + \Delta c_{\mathrm{B}}$ to be small. The small-signal assumption aligns with the operation of wearable and implantable devices, which typically track minor, continuous deviations from physiological baselines. Nevertheless, comparisons with PNP numerical simulations confirmed that the analytical model has reasonable accuracy (within ~20% error) even for large perturbations up to 90% of the initial concentration, indicating that a 10% perturbation is a conservative limit for the model validity. This leads to corresponding perturbations in the potentials: $\psi_{\mathrm{m}} \to \psi_{\mathrm{m}} + \Delta\psi_{\mathrm{diff}}$ and $\psi_0 \to \psi_0 + \Delta\psi_{\mathrm{diff}}$. In other words, we assume (as verified by PNP simulations) that both potentials shift by the same quantity $\Delta\psi_{\mathrm{diff}}$ during the diffusion phase, so that the voltage drop in the ISM remains constant. As a result, the numerator $\mathcal{N}$ remains constant to the first order. The variation of the RHS in (30) comes entirely from the denominator $\mathcal{D}(\psi_0 + \Delta\psi_{\mathrm{diff}})$.

Differentiating the equation:

$$\frac{\Delta(\text{LHS})}{\text{LHS}} = \frac{\Delta c_{\text{B}}}{c_{\text{B}}}. \tag{31}$$

For the RHS, we linearize the denominator $\mathcal{D}(\psi_0+\Delta\psi_{\text{diff}}) \approx \mathcal{D}(\psi_0) + \mathcal{D}'(\psi_0)\Delta\psi_{\text{diff}}$. This gives:

$$\frac{\Delta(\text{RHS})}{\text{RHS}} \approx -\frac{\mathcal{D}'(\psi_0)}{\mathcal{D}(\psi_0)}\Delta\psi_{\text{diff}}. \tag{32}$$

Equating the relative changes yields:

$$\frac{\Delta c_{\text{B}}}{c_{\text{B}}} = -\frac{\mathcal{D}'(\psi_0)}{\mathcal{D}(\psi_0)}\Delta\psi_{\text{diff}}. \tag{33}$$

Using the hyperbolic identity $\mathcal{D}(\psi_0) = 4\sinh^2(\psi_0/(2V_{\text{th}}))$, and differentiating with respect to ψ_0, we obtain

$$\mathcal{D}'(\psi_0) = \frac{4}{V_{\text{th}}}\sinh\left(\frac{\psi_0}{2V_{\text{th}}}\right)\cosh\left(\frac{\psi_0}{2V_{\text{th}}}\right). \tag{34}$$

Dividing by $\mathcal{D}(\psi_0)$ one gets

$$\frac{\mathcal{D}'}{\mathcal{D}} = \frac{1}{V_{\text{th}}}\coth\left(\frac{\psi_0}{2V_{\text{th}}}\right). \tag{35}$$

Substituting (35) back in (33) yields the relationship between the concentration change and the potential shift:

$$\frac{\Delta c_{\text{B}}}{c_{\text{B}}} = -\frac{1}{V_{\text{th}}}\coth\left(\frac{\psi_0}{2V_{\text{th}}}\right)\Delta\psi_{\text{diff}}. \tag{36}$$

The total Nernstian potential change is $\Delta\psi_{\text{tot}} \approx V_{\text{th}}(\Delta c_{\text{B}}/c_{\text{B}})$. Rearranging (36) allows one to compute the ratio:

$$\left|\frac{\Delta\psi_{\text{diff}}}{\Delta\psi_{\text{tot}}}\right| = \tanh\left(\frac{\psi_0}{2V_{\text{th}}}\right), \tag{37}$$

that is the split factor γ introduced in (18).

APPENDIX III
INTERFACE CONCENTRATION OVERSHOOT

This appendix focuses on the concentration overshoot at the interface, Δc_{ITF}, after the perturbation Δc_{B} in the bulk of the electrolyte. Using the relationship $c_{\text{ITF}} = c_{\text{B}}e^{-\psi_0/V_{\text{th}}}$, at the end of the diffusion phase, one has

$$c_{\text{ITF}} + \Delta c_{\text{ITF}} = (c_{\text{B}} + \Delta c_{\text{B}})\exp\left(-\frac{\psi_0 + \Delta\psi_{\text{diff}}}{V_{\text{th}}}\right), \tag{38}$$

where we have considered that at the beginning of the rate-limited phase the bulk of the electrolyte has already moved to $c_{\text{B}} + \Delta c_{\text{B}}$ while the interface potential has varied by $\Delta\psi_{\text{diff}}$ w.r.t. the value ψ_0 prior to the application of the concentration step in the bulk electrolyte.

Factoring out the equilibrium term, one gets

$$c_{\text{ITF}} + \Delta c_{\text{ITF}} = c_{\text{B}}e^{-\frac{\psi_0}{V_{\text{th}}}}\left(1 + \frac{\Delta c_{\text{B}}}{c_{\text{B}}}\right)e^{-\frac{\Delta\psi_{\text{diff}}}{V_{\text{th}}}}. \tag{39}$$

Using the first-order approximation $e^{-x} \approx 1-x$ and neglecting second-order terms ($\Delta c_{\text{B}}\Delta\psi_{\text{diff}}$), we obtain

$$c_{\text{ITF}} + \Delta c_{\text{ITF}} \approx c_{\text{ITF}}\left(1 + \frac{\Delta c_{\text{B}}}{c_{\text{B}}} - \frac{\Delta\psi_{\text{diff}}}{V_{\text{th}}}\right). \tag{40}$$

Thus, the relative change is:

$$\frac{\Delta c_{\text{ITF}}}{c_{\text{ITF}}} \approx \frac{\Delta c_{\text{B}}}{c_{\text{B}}} - \frac{\Delta\psi_{\text{diff}}}{V_{\text{th}}}. \tag{41}$$

Substituting $\Delta\psi_{\text{diff}}$ from (36):

$$\frac{\Delta c_{\text{ITF}}}{c_{\text{ITF}}} \approx \frac{\Delta c_{\text{B}}}{c_{\text{B}}}\left[1 + \tanh\left(\frac{\psi_0}{2V_{\text{th}}}\right)\right]. \tag{42}$$

Using the identity $1+\tanh(x) = \frac{2e^{2x}}{e^{2x}+1}$ (where $x = \psi_0/2V_{\text{th}}$), and remembering that $e^{\psi_0/V_{\text{th}}} = c_{\text{B}}/c_{\text{ITF}}$:

$$1 + \tanh\left(\frac{\psi_0}{2V_{\text{th}}}\right) = \frac{2}{1+e^{-\psi_0/V_{\text{th}}}} = \frac{2}{1 + c_{\text{ITF}}/c_{\text{B}}}. \tag{43}$$

Substituting this back yields the final expression:

$$\Delta c_{\text{ITF}} \approx 2\Delta c_{\text{B}}\frac{c_{\text{ITF}}}{c_{\text{ITF}} + c_{\text{B}}} \approx 2\Delta c_{\text{B}}. \tag{44}$$

since $c_{\text{ITF}} \gg c_{\text{B}}$. The validity of this analysis is verified by the PNP results in Fig. 10.

ACKNOWLEDGMENT

Prof. Alam acknowledges the support of the funding from Jai N. Gupta Distinguished Chair professorship at Purdue University, West Lafayette, Indiana, USA. The authors acknowledge the use of Google Gemini to aid the design of the graphical abstract.

REFERENCES

[1] J. Go and M. A. Alam, "The future scalability of ph-based genome sequencers: A theoretical perspective," *Journal of Applied Physics*, vol. 114, no. 16, p. 164311, 10 2013. [Online]. Available: https://doi.org/10.1063/1.4825119

[2] M. A. Alam, A. Saha, and M. Fratus, "Reliable sensing with unreliable sensors: Rethinking the theoretical foundation of field-deployed wearable/implantable/environmental sensors," *Innovation and Emerging Technologies*, vol. 9, p. 2240003, 2022.

[3] X. Jin, A. Saha, H. Jiang, M. R. Oduncu, Q. Yang, S. Sedaghat, K. Maize, J. P. Allebach, A. Shakouri, N. Glassmaker *et al.*, "Steady-state and transient performance of ion-sensitive electrodes suitable for wearable and implantable electro-chemical sensing," *IEEE Transactions on Biomedical Engineering*, vol. 69, no. 1, pp. 96–107, 2021.

[4] A. Saha, S. Sedaghat, S. Gopalakrishnan, J. Waimin, A. Yermembetova, N. Glassmaker, C. Mousoulis, A. Shakouri, A. Wei, R. Rahimi *et al.*, "A new paradigm of reliable sensing with field-deployed electrochemical sensors integrating data redundancy and source credibility," *Scientific Reports*, vol. 13, no. 1, p. 3101, 2023.

[5] A. Saha and M. A. Alam, "A real-time self-powered equivalent circuit extraction technique to monitor the degradation of a field-deployable ise," *ACS Sensors*, vol. 10, no. 11, pp. 8966–8974, 2025, pMID: 41128010. [Online]. Available: https://doi.org/10.1021/acssensors.5c03094

[6] M. Fratus, J. Lim, J. K. Nolan, E. Madsen, Y. Dai, C. H. Lee, J. C. Linnes, H. Lee, and M. A. Alam, "Geometry-defined response time and sensitivity for microneedle-based amperometric sensors," *IEEE Sensors Journal*, vol. 23, no. 13, pp. 14 285–14 294, 2023.

[7] M. Fratus and M. A. Alam, "Can we still use the michaelis–menten model for enzymatic microneedle sensors?" *Proceedings of the National Academy of Sciences*, vol. 122, no. 30, p. e2418168122, 2025.

[8] W. Morf, E. Pretsch, and N. De Rooij, "Computer simulation of ion-selective membrane electrodes and related systems by finite-difference procedures," *Journal of Electroanalytical Chemistry*, vol. 602, no. 1, pp. 43–54, 2007. [Online]. Available: https://www.sciencedirect.com/science/article/pii/S0022072806006711

[9] D. Yuan and E. Bakker, "Overcoming pitfalls in boundary elements calculations with computer simulations of ion selective membrane electrodes," *Analytical Chemistry*, vol. 89, no. 15, pp. 7828–7831, 2017, pMID: 28699340.

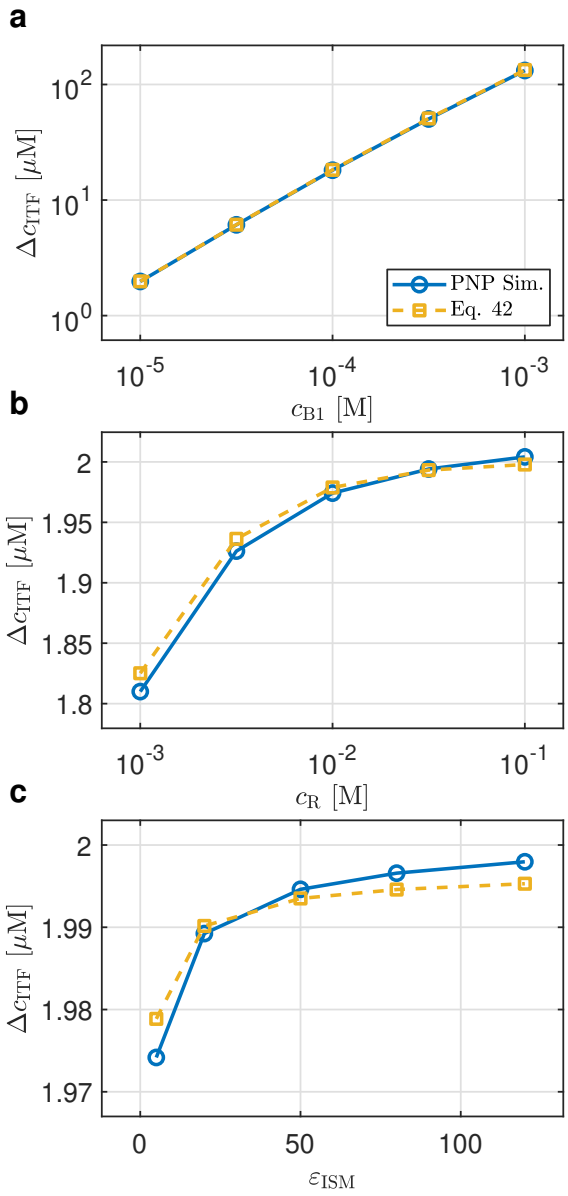

Fig. 10. Validation of the analytical model for the interface concentration overshoot, $\Delta c_{\mathrm{ITF}} \simeq 2\Delta c_{\mathrm{B}}$. **a)** Sweep of bulk concentration c_{B1} (with $c_{\mathrm{R}} = 10$ mM and $\varepsilon_{\mathrm{ISM}} = 5$). **b)** Sweep of fixed ionic site concentration c_{R} (with $c_{\mathrm{B1}} = 10$ μM). **c)** Sweep of membrane dielectric constant $\varepsilon_{\mathrm{ISM}}$ (with $c_{\mathrm{B1}} = 10$ μM and $c_{\mathrm{R}} = 10$ mM). PNP simulation results (solid lines with circles) show excellent agreement with predictions from (44) (dashed/dotted lines). In all cases, $\Delta c_{I,B}$ of 10% of c_{B1} was used.

[10] B. Hambly, M. Guzinski, B. Pendley, and E. Lindner, "Kinetic description of the membrane–solution interface for ion-selective electrodes," *ACS Sensors*, vol. 5, no. 7, pp. 2146–2154, 2020, pMID: 32560587.

[11] L. J. Mele, P. Palestri, L. Selmi, and M. A. Alam, "Modeling non-equilibrium ion-transport in ion-selective-membrane/electrolyte interfaces for electrochemical potentiometric sensors," *IEEE Sensors Journal*, vol. 22, no. 13, pp. 12 987–12 996, 2022.

[12] P. Bergveld, "A critical evaluation of direct electrical protein detection methods," *Biosensors and Bioelectronics*, vol. 6, no. 1, pp. 55–72, 1991.

[13] H.-C. Chang and G. Jaffé, "Polarization in electrolytic solutions. Part I. Theory," *The Journal of Chemical Physics*, vol. 20, no. 7, pp. 1071–1077, 1952, doi: 10.1063/1.1700669.

[14] *Introduction: Principles and Concepts*. New York, NY: Springer New York, 2008, pp. 1–10. [Online]. Available: https://doi.org/10.1007/978-0-387-75936-4_1

[15] L. J. Mele, P. Palestri, M. A. Alam, and L. Selmi, "Selectivity, sensitivity and detection range in ion-selective membrane-based electrochemical potentiometric sensors analyzed with poisson-boltzmann equilibrium model," *IEEE Sensors Journal*, vol. 22, no. 15, pp. 15 010–15 021, 2022.

[16] Y. Dai, J. Nolan, E. Madsen, M. Fratus, J. Lee, J. Zhang, J. Lim, S. Hong, M. A. Alam, J. C. Linnes, H. Lee, and C. H. Lee, "Wearable sensor patch with hydrogel microneedles for in situ analysis of interstitial fluid," *ACS Applied Materials & Interfaces*, vol. 15, no. 49, pp. 56 760–56 773, 2023, pMID: 38041570.

[17] M. Fratus and M. A. Alam, "Theory of nanostructured sensors integrated in/on microneedles for diagnostics and therapy," *Biosensors and Bioelectronics*, vol. 255, p. 116238, 2024. [Online]. Available: https://www.sciencedirect.com/science/article/pii/S0956566324002434

[18] A. Moudgil, K. Hou, T. Li, and W. L. Leong, "Biocompatible solid-state ion-sensitive organic electrochemical transistor for physiological multi-ions sensing," *Advanced Materials Technologies*, vol. 8, no. 18, p. 2300605, 2023.

[19] A. Moudgil and W. L. Leong, "Highly sensitive transistor sensor for biochemical sensing and health monitoring applications: A review," *IEEE Sensors Journal*, vol. 23, no. 8, pp. 8028–8041, 2023.